Matthews, M., Kearns, S., & Buse, B. (2018). Electron Beam-Induce Carbon Erosion and the Impact on Electron Probe Microanalysis. *Microscopy and Microanalysis*. https://doi.org/10.1017/S1431927618015398

Electron Beam Induced Carbon Erosion and the Impact on Electron Probe Microanalysis

Mike B. Matthews[1,2], Stuart L. Kearns[2] and Ben Buse[2]

[1]AWE, Aldermaston, Reading, RG7 4PR, UK

[2]University of Bristol, School of Earth Sciences, Wills Memorial Building, Queens Road, Clifton, BS8 1RJ, UK

Abstract

Electron beam induced carbon contamination is a balance between simultaneous deposition and erosion processes. Net erosion rates for a 25nA 3kV beam can reduce a 5nm C coating by 20% in 60s. Measurements were made on C coated Bi substrates, with coating thicknesses of 5 – 20nm, over a range of analysis conditions. Erosion showed a step-like increase with increasing electron flux density. Both the erosion rate and its rate of change increase with decreasing accelerating voltage. As the flux density decreases the rate of change increases more rapidly with decreasing voltage.

Time Dependent Intensity (TDI) measurements can be used to correct for errors, in both coating and substrate quantifications, resulting from carbon erosion. Uncorrected analyses showed increasing errors in coating thickness with decreasing accelerating voltage. Whilst the erosion rate was found to be independent of coating thickness this produces an increasing absolute error with decreasing starting thickness, ranging from 1.5% for a 20nm C coating on Bi at 15kV to 14% for a 5nm coating at 3kV. Errors in Bi Mα measurement are <1% at 5kV or above but increase rapidly below this both with decreasing voltage and increasing coating thickness to 20% for a 20nm coated sample at 3kV.

Introduction

C is predominantly the coating material of choice for electron probe microanalysis: Its low atomic number, and consequently generally low absorption of both electrons and X-rays, means that it can normally be considered an insignificant component of analysis; it has one x-ray emission line which generally does not interfere with other elements of interest; it is easy to apply in thin, consistent and electrically conductive layers; it is cheap. At low accelerating voltages, however, even a thin C coating can become a significant component of the analysis volume: At 5kV a 20nm C coating will reduce the Lα emission from a Bi substrate by 10% (Matthews et al. 2018a).

However, regardless of the coating material used, C contamination build-up is a known issue in electron microanalysis, forming ring-shaped contamination deposits (e.g. Buse & Kearns, 2015; Reimer & Wachter, 1978) several microns wider than the beam diameter (Silvis-Cividjian et al. 2002). The lateral extent of the contamination spots produce changing coating thicknesses not just under the beam analysis spot but for consecutive analyses when small point spacings are used. Indeed, the ring-shaped topography typical of these contamination build-ups has a more adverse effect on subsequent closely adjacent analyses than on the analysis point forming the initial contamination (Buse & Kearns 2015).

What is less commonly reported in microanalysis studies is erosion of C by the electron beam. Heide (1962) measured erosion rates of up to 1nms^{-1}, although this was at sub-ambient temperatures. Figure 1a shows a backscatter electron (BSE) image of a single contamination spot formed by a static focussed electron beam, approximately 100nm diameter, on a carbon coated Bi sample. The classic ring-shaped contamination morphology can clearly be seen, extending to a diameter of ~2μm. However, the centre of the contamination appears brighter in this BSE image than the surrounding uncontaminated sample, which is confirmed by the brightness profile plot shown in Figure 1b. The increased BSE brightness is caused by partial erosion of the C coat, locally increasing the mean atomic number and thereby the backscatter coefficient. Where the C is present as contamination erosion may be advantageous if the contamination can be removed entirely, but where it is not fully removed, or where the C being eroded is the conductive coating, this effect can be as deleterious as contamination build up since it changes the surface coating thickness. In this study we investigate the factors that influence when erosion occurs, how it can be mitigated, measure the rates of erosion, propose what factors affect the rate, and characterise the potential impact on quantification of the sample beneath the conductive coat.

The results reported here are for C coated Bi samples. These form part of a wider study on the microanalysis of nuclear materials, with Bi acting as a heavy metal non-radioactive surrogate for U and Pu. However, the results presented are equally applicable to other materials.

a)

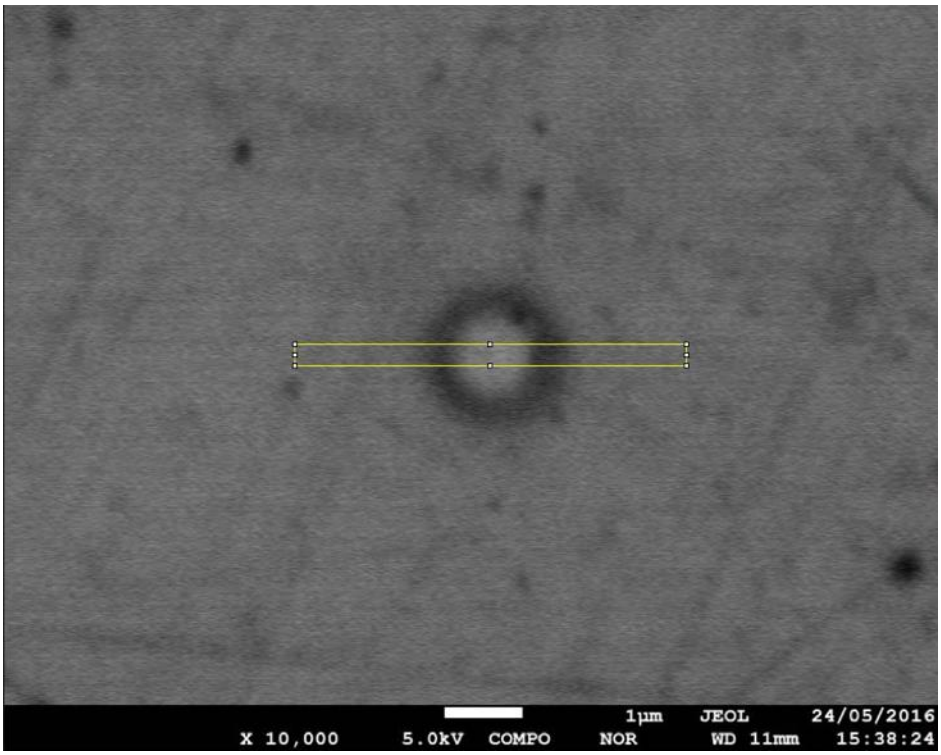

b)

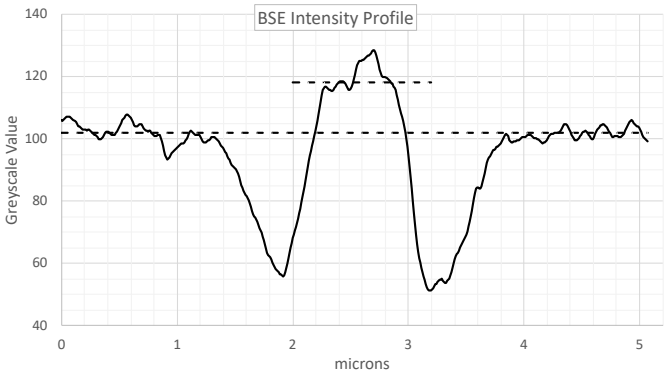

Figure 1 *a) BSE image of a contamination spot formed by a static focussed electron beam, approximately 100nm in diameter, on a carbon coated Bi sample.*
b) Image brightness profile across the contamination spot as measured along the yellow region shown in a).

Materials and Methods

Four samples of Bi metal were mounted in conducting Bakelite, ground and polished with SiC papers and diamond suspensions respectively to a final grade of 1μm in oils suspension. A combination of propanol followed by a rinse with ethanol was found to be the most effective way to wash off the polishing oil and leave a residue free surface. This is in agreement with (Pinard 2016) who carried out an in-depth comparison of the carbon surface residues left by different solvents and measured the lowest levels for ethanol, methanol and petroleum benzene. The cleaned polished faces were then C coated in a Leica ACE600 coater (Leica Microsystems Ltd., Milton Keynes, UK), with a C-cord source, to target thicknesses of 5, 10, 15 and 20nm. The deposited thicknesses, as measured using a Film Thickness Monitor (FTM) sensor co-located with the samples, were 5.06, 10.08, 15.10 and 20.28nm. For brevity the four samples will be referred to using their nominal thicknesses in single quotes (e.g. '5nm') unless the absolute thickness is being referenced.

Analyses were carried out in a JEOL JXA-8530F (JEOL Ltd., Tokyo, Japan)field emission gun electron microprobe (FEG-EPMA) at the University of Bristol, using Probe for EPMA acquisition and processing software (Probe Software Inc., Eugene, USA). Table 1 Spectrometer configurations used for analyses.

summarises the spectrometer configuration used for all the analyses. On each sample 3x4 arrays of points were acquired at 3, 3.4, 5, 7, 10 and 15kV. The C Kα and Bi Mα peak positions were determined on vitreous C and Bi-metal respectively. To measure changes in x-ray intensity during analysis the Time Dependent Intensity (TDI) mode was used. This method has been applied in the past to correct for beam induced changes in sample chemistry, for example for Na migration in glasses (Nielsen & Sigurdsson 1981) and F and Cl diffusion in apatites (Stormer et al. 1993). This analysis mode sub-divides the counting time into intervals, with the counts recorded for each. Results can then be output either as total measured counts (no TDI correction) or calculated by extrapolating the interval intensities back to zero time (TDI corrected). For this study the peak counting times were divided into 6 x 10s intervals on peak, and 10s on each of two background positions per element.

	Sp1	Sp2	Sp3	Sp4	Sp5
Counter:	P10	P10	P10	Xe	Xe
Crystal:	STE	LDE2	PETH	PETH	PETL

Element:	C Kα	C Kα	Bi Mα	Bi Mα	Bi Mα

Table 1 Spectrometer configurations used for analyses.

At each accelerating voltage analyses were acquired using combinations of beam currents of 25 and 50nA and with focussed and 5μm and 10μm defocussed beams. Faraday cup measurements at the start and end of each analysis are used to correct for any drift in beam current during the analysis. This correction assumes a linear change in current between the two measured values. However, the column was found to be very stable, with only minimal changes in beam current during any given measurement period. To avoid artefacts from contamination from previous analyses a point spacing of 20μm was used for each array, and a new area of each sample was used for each accelerating voltage. For calibration uncoated Bi metal (the same batch as that used for the samples) and vitreous C, both mounted in conducting Bakelite, were used. To remove any surface oxide or contamination, the reference materials were hand polished using a 1μm diamond in oil suspension, washed with propanol and rinsed with ethanol immediately prior to loading into the EPMA for analysis. K-ratios (counts on sample/counts on reference material) were calculated for each spectrometer, and the mean values from spectrometers 1 and 2, and spectrometers 3, 4 and 5 at each point gave the final k-ratio values for C and Bi respectively.

Results

Error! Reference source not found.a shows example TDI plots for the '5nm' C on Bi sample, acquired at 5kV with a 50nA for a focussed beam and for 5μm and 10μm defocussed beams. For each of the three data sets the mean and 1σ standard deviation has been calculated from the 3x4 array of points for each time interval. The dashed lines are linear fits through the means and indicate the extrapolations back to zero time. The focussed and 5μm defocussed beam data sets show very similar behaviours, with linear changes in intensity with time, and having similar total decreases in intensity (and therefore rate of decrease with time). Note that the intensities are given in counts per second per nano-amp (cps/nA) so have been corrected for any beam current drift. The final measured intensities in both cases show ~15% decrease relative to the extrapolated zero-time intensities, consistent with the erosion of carbon under the electron beam (see Figure 1). The 10μm defocussed beam data also shows a linear trend, but with a significantly reduced rate of C intensity decrease. For comparison, Figure 2b shows similar plots for an uncoated Bi sample. These show constant C Kα signals, representing the background signal level with no accumulation or loss of C in the form of hydrocarbon contamination – possibly reflecting the cleanness of the sample.

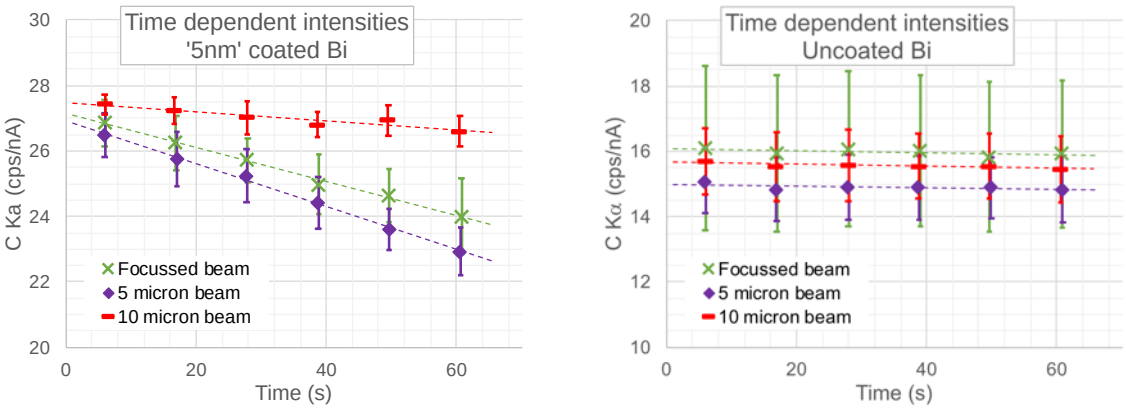

a b

Figure 2 *Plots of the means and 1σ standard deviations of the C Kα TDI measured intensities for a) the '5nm' C coat on Bi sample and b) the uncoated Bi reference material, both analysed at 5kV and 50nA with a focussed beam and with 5μm and 10μm defocussed beams. The dashed lines are linear fits through the mean values.*

Smaller but correlated increases in Bi Mα intensities were also measured for all samples that showed C intensity decreases, as would be expected for thinning C coats. For example, Figure 3 shows the TDI data for Bi Mα measured using a 5μm defocussed beam.

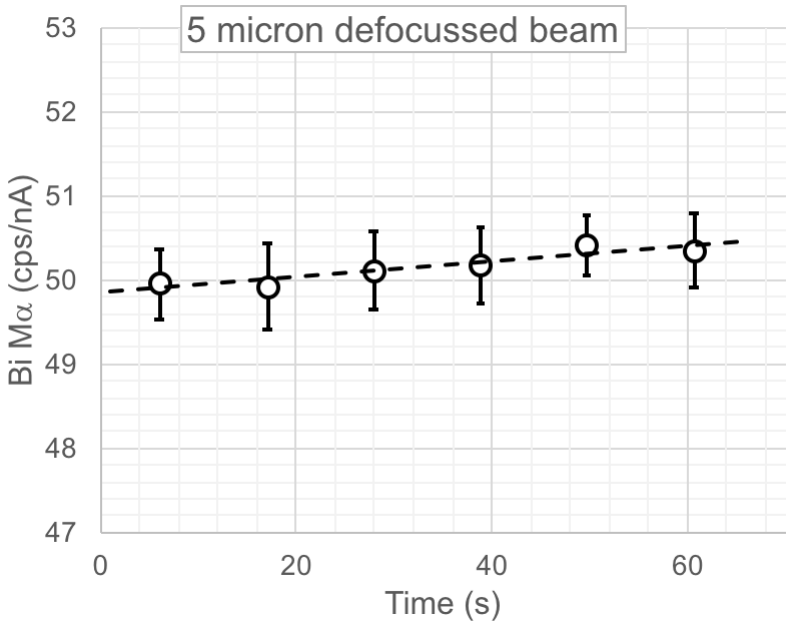

Figure 3 *Plot of the means and 1σ standard deviations of the Bi Mα TDI measured intensities for the '5nm' C coat on Bi sample, analysed at 5kV and 50nA with a 5μm defocussed beam. The dashed line is the linear fit through the means.*

Discussion

Factors Affecting Carbon Deposition and Erosion

The mechanism for contamination deposition in the electron microscope is reasonably well understood, largely due to advances in the field of Electron Beam Induced Deposition (EBID). Deposition of hydrocarbons or other molecules are controlled by the same processes. Utke et al. (2008) and Hren (1979) provide comprehensive reviews of the methods and mechanisms of both deposition and erosion processes. Secondary electrons

have energies in the range where molecules absorbed to the sample surface (e.g. hydrocarbons) typically have a peak in their dissociation cross-sections, in the range 20 – 50V (van Dorp et al. 2005). As the SEs are emitted from the sample they can thus decompose hydrocarbons (or other absorbed molecules) into volatile and non-volatile components (Choi et al. 2006). The former are pumped away by the vacuum system and the latter are deposited on any nearby surface. In the EBID lithographic technique a precursor gas containing the required deposit is injected in the region of the beam impact point to provide an essentially limitless supply of the required deposit. For example, in Focussed Ion Beam (FIB) sample preparation a Pt-bearing precursor gas and an electron beam can be used to apply a 'strap' of Pt on the selected area of a sample (Choi et al. 2006) to preserve the surface during subsequent ion milling. EBID depositions, under high vacuum, for a fixed focussed beam typically form a sharp central peak, marginally larger than the primary beam diameter, surrounded by a disk which is considerably wider than the primary beam (Silvis-Cividjian et al. 2002). Toth et al. (2007) explicitly linked the central pillar and wide disk components of contamination deposition to type I and type II secondary electrons (SE-I and SE-II) respectively. SE-I are generated directly by the primary electron beam and are emitted from a diameter only ~1nm wider than that of the electron beam. Type II SE are predominantly generated by the much wider spread backscatter electrons (BSE) and consequently can be emitted significantly further from the beam impact point. This can be seen from the ~2μm diameter contamination spot shown in Figure 1a which was formed by a fully focussed beam of perhaps 100nm diameter. This proposed mechanism is corroborated by contamination formed under TEM-type analysis conditions, i.e. high accelerating voltages and thin samples. Under these conditions the primary beam undergoes little scattering as it passes through the sample, BSE and SE-II emission is minimal, and only the central peak feature of contamination is formed (e.g. Lobo et al. 2008; Tanaka et al. 2005; van Dorp et al. 2005; Shimojo et al. 2004). The rate of deposition can be increased by reducing the primary beam accelerating voltage (Kohlmann-von Platen & Bruenger 1996), or by increasing the electron flux density (Amman et al. 1996). Modelling of the surface BSE distributions as functions of accelerating voltage shows that the diameter of contamination should increase with increasing voltage although Amman et al. (1996) reported that the diameter of contamination was independent of deposition rate. Figure 4 shows the BSE intensities per unit area as functions of radial distance and accelerating voltage for a Bi sample coated with 20nm of C, modelled with Casino v2.51. This shows that the radial extent increases with accelerating voltage. The number of electrons per unit area decreases very rapidly with increasing distance from the primary beam. Thus the radius at which there are insufficient electrons to crack the hydrocarbons and produce detectable contamination may well result in a much smaller change in contamination area with voltage. Investigation of what the intensity threshold level is falls outside the scope of this study.

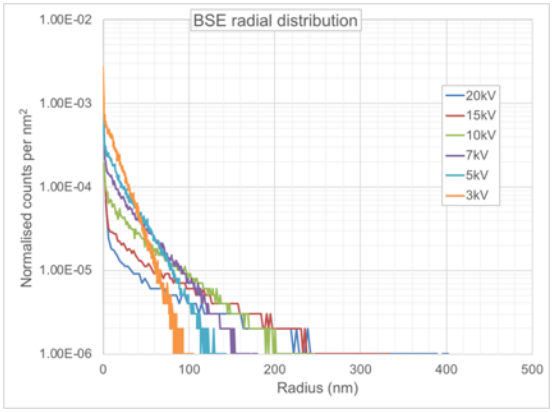

Figure 4 *Modelled radial BSE counts per unit area as functions of radial distance from the primary beam and accelerating voltage for a 20nm C film on a Bi substrate, using Casino v2.51.*

Whilst in the past vacuum oils and greases were identified as the main sources of contamination (e.g. Ennos 1953; Ennos 1954), Amman et al. (1996) experimentally demonstrated that the primary source of hydrocarbons in a modern SEM was the sample surface and not the analysis chamber atmosphere: By pulsing the electron beam at different frequencies they were able to show that the supply of hydrocarbons becomes locally depleted if the duration of the pulsing is less than ~3s, and link this to the surface diffusion rate of hydrocarbons. This is supported by modelling of the deposition mechanism (e.g. Choi et al. 2006; Utke et al. 2008), and by the effectiveness of plasma cleaning of samples prior to analysis for reducing the degree of contamination (e.g. Isabell et al. 1999; Mitchell 2015).

In the EBID-related lithographic technique of Electron Beam Induce Erosion (EBIE), the gas injected is oxygen-bearing, for example air or H_2O. This promotes volatilisation of the surface under the electron beam, with erosion occurring primarily directly under the primary electron beam. Amman et al. (1996) demonstrated that both C erosion and deposition can occur simultaneously. They experimentally demonstrated that, as the rate of erosion increases relative to the rate of deposition, the central peak reduces, then disappears, and finally the disk becomes a hollow ring (i.e. the form typically seen in electron microanalysis). They link the rate of erosion to electron flux density, temperature, precursor partial pressure, and dissociation cross-section. Lobo et al. (2008) modelling of the balance between deposition and erosion shows that, once erosion dominates in the central region, increasing the electron flux increases the diameter of the erosion area. It has been proposed that beam induced heating promotes erosion (e.g. Bastin & Heijligers 1988) but Toth et al. (2007) argue that the sub-micron transitions from erosion to deposition (as shown by the BSE profile in Figure 1b) are too small for even the steepest possible thermal gradients. Also, Heide (1962) found that erosion increased as the sample temperature was decreased rather than increased, measuring an erosion rate of $1nms^{-1}$ at a sample temperature of -120°C.

In order to test for correlations between the rate of C erosion and the parameters varied across the data sets for this study the C erosion rate was determined for each analysis point. This was calculated in terms of the change in measured C Kα X-ray intensity per unit time of beam exposure, in counts per second per nano-amp per second (cps/nA/s) using the TDI data for each analysis point. Figure 5 Changes in C Kα measured intensity on spectrometer 2 plotted as functions of a) the electron flux density, b) the beam diameter, and c) deposited coating thickness as measured using the FTM. The horizontal black bars and the vertical

lines represent the mean and 1σ standard deviation values for each data set. shows the mean values and 1σ standard deviation error bars of the measured C Kα intensities plotted as functions of (a) the electron flux density, (b) the beam diameter, and (c) deposited coating thickness. A beam diameter of 100nm was assumed to calculate the flux density for the fully focussed beam analyses, based on previous measurements on this instrument of the change in SE intensity across sharp edged sample features. Pinard (2016) calculated theoretical beam diameter values as functions of accelerating voltage and probe current for a Schottky FEG-EPMA. Extrapolating between his plotted curves gives a range of approximately 50 – 100nm over the range of analysis conditions used in this study. The large error bars show there is a considerable degree of scatter in most of the datasets, and a correlation between erosion rate and electron flux density, as found by Amman et al. (1996), is not obvious in Figure 5a. Here mean erosions rates of approximately 0.05 cps/nA/s are measured at flux densities of 1nA/μm^2 or higher, whilst below 1nA/μm^2 they reduce to only about 0.01cps/nA/s. Similarly, the beam diameter at a given accelerating voltage (Figure 5 Changes in C Kα measured intensity on spectrometer 2 plotted as functions of a) the electron flux density, b) the beam diameter, and c) deposited coating thickness as measured using the FTM. The horizontal black bars and the vertical lines represent the mean and 1σ standard deviation values for each data set.b) indicates a similar change behaviour, with comparable erosion rates for the 5μm defocussed and the fully focussed beam and both a significantly lower mean erosion rate and lower degree of scatter for the 10μm defocussed beam. There is no evident effect of the starting coating thickness on the C erosion rate (Figure 5c). It's interesting to note the significantly lower degree of scatter in the measurements on the uncoated Bi reference sample (the zero coating thickness data points in Figure 5c). Since this sample is uncoated this scatter can be used to give an indication of the noise or counting error relating to the measurement of the C Kα intensities. The very large range of variations seen in many of the measurements of the coated samples must therefore represent at least a degree of variation in the measured erosion rates. This is discussed further below.

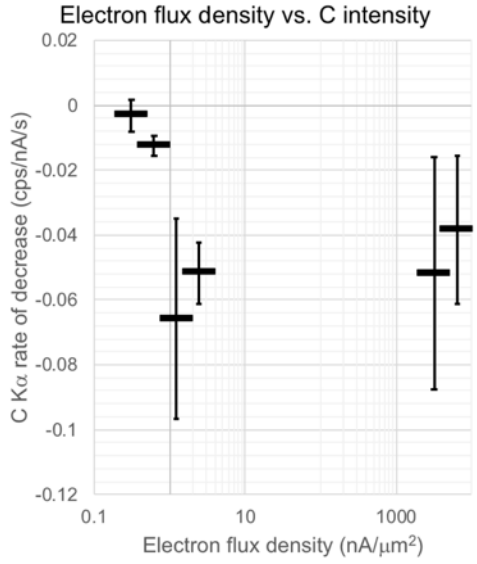

a)

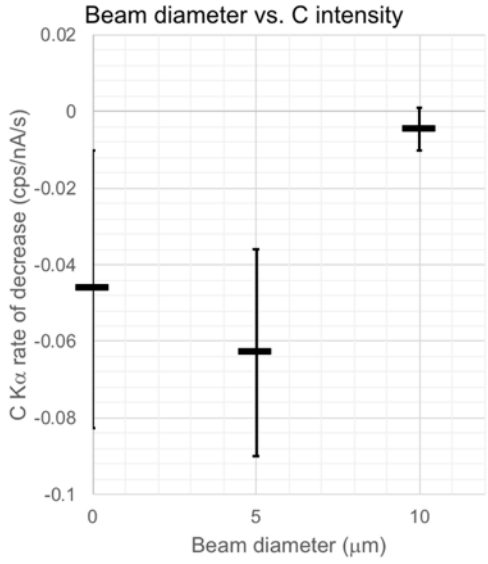

b)

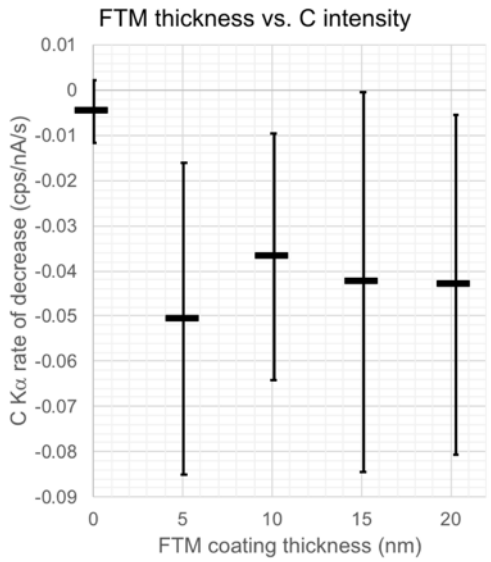

c)

Figure 5 Changes in C Kα measured intensity on spectrometer 2 plotted as functions of a) the electron flux density, b) the beam diameter, and c) deposited coating thickness as measured using the FTM. The horizontal black bars and the vertical lines represent the mean and 1σ standard deviation values for each data set.

Figure 6 shows the C erosion rate plotted as a function of both the accelerating voltage and the beam diameter and here we see a more significant trend; the data for the 5μm defocussed beam in Figure 6b shows an increase in erosion rate with decreasing accelerating voltage, matching the behaviour for C deposition found by Kohlmann-von Platen & Bruenger (1996). The trend is not linear, with the rate of change also increasing as the accelerating voltage decreases (indicated by the curve of the dashed line which has been manually drawn through the data points in each plot). A similar but more extreme behaviour is seen in the data for the 10μm defocussed beam (Figure 6Figure 6 Changes in C Kα measured intensity on spectrometer 2 plotted as functions of the accelerating voltage for a) fully focussed, b) 5μm defocussed, and c) 10μm defocussed beams. The dashed lines indicate the trends of the maximum erosion rates as a function of accelerating voltage in each plot. The flux densities for the three plots are approximately 3200, 1.2 and 0.3nA/μm^2 respectively.

c), with the maximum measured erosion rate initially decreasing sharply with increasing voltage but the rate of change rapidly reduces as the erosion rate reaches zero by 10kV. The data for the fully focussed beam (Figure 6a) is less clear: At 7kV and above the data is consistent with the trends in the two defocussed beam datasets, with the erosion rate increasing with decreasing voltage but with a decreasing curvature in the rate of change as the beam diameter decreases. However, at 5kV and below the degree of scatter in the data increases dramatically. The maximum measured erosion rates fit the same trend as the 7, 10 and 15kV data points, but there are a significant number of data points showing much lower erosion rates, and even one data point showing net deposition.

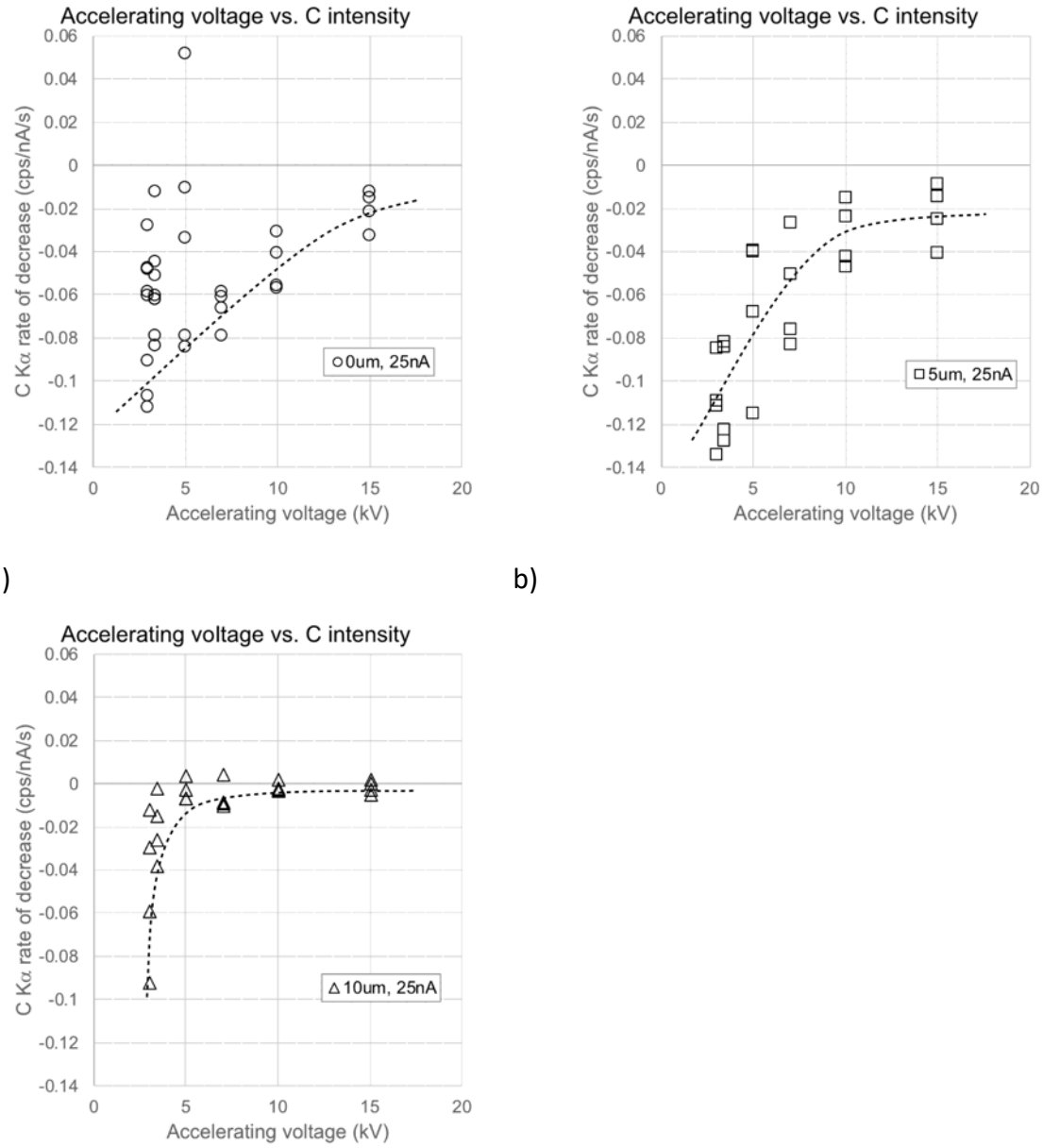

Figure 6 *Changes in C Kα measured intensity on spectrometer 2 plotted as functions of the accelerating voltage for a) fully focussed, b) 5μm defocussed, and c) 10μm defocussed beams. The dashed lines indicate the trends of the maximum erosion rates as a function of accelerating voltage in each plot. The flux densities for the three plots are approximately 3200, 1.2 and 0.3nA/μm^2 respectively.*

The correlation with accelerating voltage is compatible with the erosion being caused by SE-I emissions: As the voltage is decreased the depth of the interaction volume decreases and, since a higher proportion of the interactions move closer to the surface, a higher proportion of SE's are emitted. Figure 7 shows that, over the range of voltages commonly experienced in EPMA, the increase in SE yield with decreasing accelerating voltage for a Bi sample coated with 10nm of C from 2 – 20kV, calculated using Casino v3.3.0.4 (Demers et al. 2011), with 10,000 electron trajectories and a 50eV low energy cut-off at all accelerating voltages. Reimer & Tollkamp (1980) measured a large range of elements and showed that all show similar trends. Similarly for deposition, as the voltage decreases the surface expression of

the analysis volume decreases so the BSE's and SE-II's are emitted from a smaller area. Thus, as the accelerating voltage is decreased the emitted flux densities of both SE-I and SE-II increase.

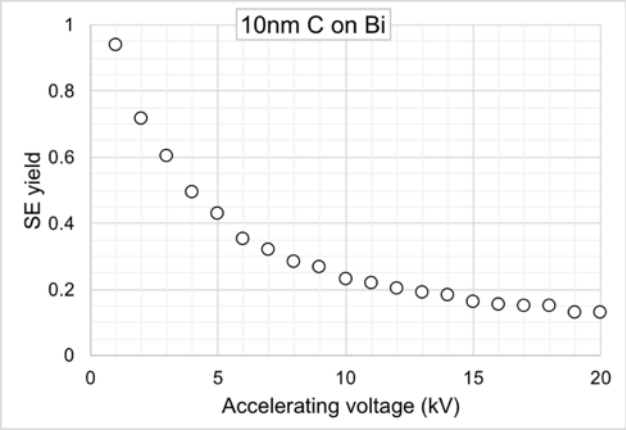

Figure 7 *Secondary electron yield as a function of accelerating voltage for a Bi substrate with a 10nm C coating. Calculated using WinCasino3_x64.*

The behaviour of the erosion rates shown in Figure 5 and Figure 6 can be explained by the change in balance between erosion and deposition as the accelerating voltage decreases. Toth et al (2007) argued that the measured erosion/deposition rate at any given point is the balance between competing simultaneous removal and accumulation processes. Both will increase as the accelerating voltage decreases but, since the deposition rate is ultimately limited by the surface diffusion rate of source hydrocarbons (Amman et al. 1996) the erosion rate will rapidly dominate. This produces the apparent step change in erosion rate as a function of flux density and beam diameter, as seen in Figure 5a and b respectively. The changes in both accelerating voltage and beam diameter in Figure 6 show that the change in erosion rate is in fact progressive, but that the rate of change can be rapid for relatively small changes in accelerating voltage.

The high degree of scatter seen for the fully focussed beam, and at low accelerating voltages can perhaps be attributed to beam positional stability: For a fully focussed beam the erosion area will be relatively small and any movement in the beam position during analysis will move the measurement point into the contamination halo where additional C has been deposited. Whilst the data shows no shifts from an eroding static beam which subsequently drifts onto the contamination halo, which would be marked by a step in the carbon Kα intensity versus time plot, continuous drift cannot be ruled out, where the beam is constantly eroding into the contamination halo. Several authors (e.g. Buse & Kearns 2015; Pinard et al. 2013) identified that a rastered beam or closely spaced stepped beam can overlap contamination halos. This could explain the larger variation seen for the coated samples relative to the uncoated sample seen in Figure 5c above. Buse & Kearns (2015) noted an increase in beam drift with poorer chamber vacuum levels. At the lower accelerating voltages it might also be expected that the positional stability is poorer compared to the higher voltages since the beam will be more sensitive to any stray electron-magnetic fields in the instrument and/or the lab, especially if the instrument is not fitted with field cancellation coils, as is the case for the EPMA used for these analyses. From the intensity plot in Figure 1b above the eroded region is sharply defined and the deposition rate in the surrounding ring is greater than the erosion rate in the centre. Thus, any drift into the deposition ring can produce a discernible change in the measured net erosion rate.

However, it's less clear that this mechanism can explain the dramatic increase in the degree of scatter measured at 5kV and below shown in Figure 6a above. Another possible mechanism is discussed below. Regardless of the cause, the degree of scatter measured makes estimation of variation in the true erosion rate more difficult. It also adds to the uncertainty in any given analysis since, even if erosion is recognised and the true erosion rate is constant at the given analysis conditions, beam drift can significantly change the measured erosion rate or even change from net erosion to net deposition.

The high noise level in X-ray count intensities makes it difficult to see any small or gradual changes in intensity during an analysis that might indicate that erosion or deposition is occurring. The red trace in **Error! Reference source not found.**a shows C Kα measurements made at 0.5s intervals on the '5nm' C coated Bi sample at 15kV with a focussed beam for a 70s total period. Although the overall decreasing trend is apparent the high noise level is also very evident, and 30 – 40s of data is needed before the decreasing trend becomes reliably identifiable. Integrating the count intervals over 10s (shown by the red diamonds) significantly improves the noise level but 20-30s still need to be acquired before an increasing or decreasing trend is revealed. In contrast the absorbed current measured at 0.5s intervals in parallel with the x-ray intensities (shown by the black line) shows changes within a few seconds. The absorbed current can be simultaneously measured during an analysis and the much lower noise level can give a readily visible indication of erosion or deposition: The high atomic number contrast between the C coating and the Bi substrate mean that any change in the C coating thickness produces a change in the BSE co-efficient and hence an opposite change in the absorbed current. For comparison, Figure 8b shows a similar plot but for an uncoated Bi. Both the x-ray counts and the absorbed current are essentially constant and again this is much more readily evident in the absorbed current trace.

It is potentially possible to calibrate the absorbed current as a function of the coating X-ray signal to take advantage of the much better signal to noise ratio. However, such a calibration would only be valid for a given sample at given analysis conditions at the time of the calibration since, even if the same sample was just moved in the sample holder, analysed under exactly the same instrument conditions, and assuming that the surface contamination hadn't changed in the process, the electrical contact with the stage, and therefore the absorbed current circuit, would almost certainly be different and the X-ray intensity versus absorbed current calibration would no longer be valid. This does not detract, though, from the value of the absorbed current as a high sensitivity and easy to use indicator of beam induced changes in the coating and where TDI analysis may be beneficial.

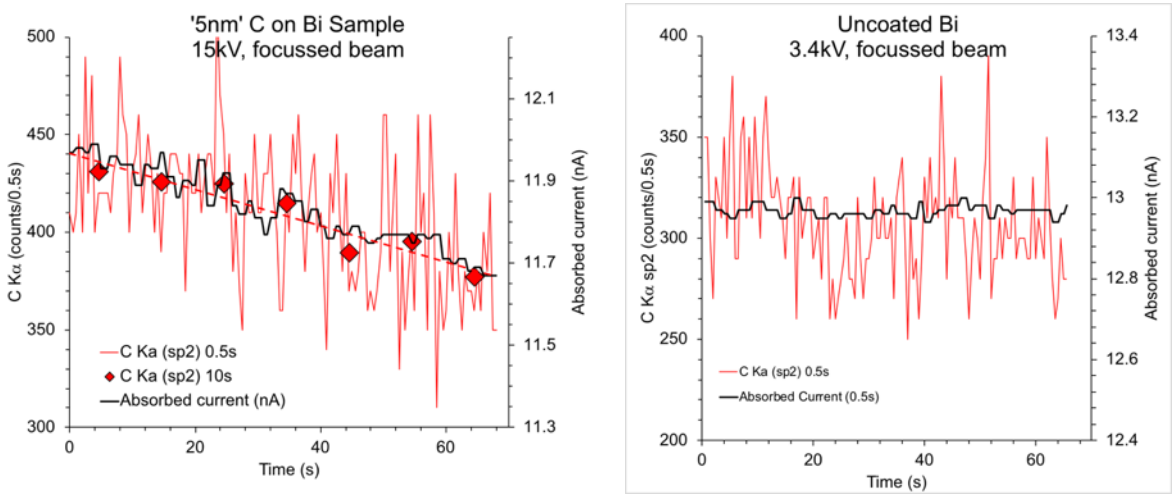

a b

Figure 8 *Comparison of change in C Kα intensity and absorbed current for a) a '5nm' C coated Bi and b) an uncoated Bi. The open circles are 0.5s interval measurements of the C Kα intensity whilst the diamonds are 10s averaged C Kα intensities. The black line is the 0.5s interval measured absorbed current.*

It's apparent from the results in this study that, at a given accelerating voltage, relatively small changes in the flux density significantly change the balance between deposition and erosion under the electron beam, matching the 'on-off type' behaviour referred to by Toth et al. (2007). At higher flux densities varying the accelerating voltage can produce more gradual changes in erosion. However, none of the conditions used in this study showed zero net erosion. A few individual analyses did show net deposition, but only at conditions where the majority of analyses showed net erosion so these few points are taken to result from higher beam drift rates rather than true net deposition conditions. Heide (1962) noted that "*the conditions under which neither contamination nor removal of carbon takes place, are very difficult to realise experimentally*". Thus, for C coated samples, the assumption that the coating thickness is constant needs to be verified rather than assumed.

The rapid change to high net erosion is related to the surface diffusion rate of source hydrocarbons limiting the maximum rate of deposition. However, it is apparent in these results that, at a given accelerating voltage the rate of erosion also appears to reach a limit. For example, at 5kV the mean measured rate of erosion does not increase with increasing flux density above 1nA/μm^2. As mentioned above, in EBIE an oxygen-bearing gas, commonly air or H_2O vapour (e.g. Kohlmann-von Platen & Bruenger 1996), is injected to drive erosion. This is why an air jet is an effective anti-contamination device. Bastin & Heijligers (1988) ingeniously used an air jet combined with a high beam current to deliberately completely erode small windows through carbon coats to allow for uncoated point analyses of insulating materials, with the surface charge being dissipated to the adjacent intact conductive coating. Toth et al. (2007) also linked the maximum rate of erosion to the supply of O_2. The rate in an SEM/EPMA then becomes a factor of the chamber vacuum level. The improvement seen in vacuum levels when liquid nitrogen traps are used in the analysis chamber (e.g. Buse et al. 2016) implies that at least the H_2O is present in the chamber atmosphere and not just adsorbed on the sample surface. The rate of erosion is therefore significantly less limited than is the deposition since diffusion rates of O_2 and H_2O in the gas phase would be expected to be significantly higher than for the surface diffusing

hydrocarbons. Bastin and Heijligers (Bastin & Heijligers 1988) demonstrated the presence of oxygen in the analysis chamber by measuring detectable levels on pure Au: Since Au has no solubility for oxygen any measured levels must be adsorbed onto the surface from the chamber atmosphere. They also found that nitrides showed slow increases in oxygen during long period analyses and concluded that the beam was inducing in-situ oxidation. Thus, even without an air jet, the vacuum level in a typical EPMA or SEM is low enough that the remaining air/H_2O, in combination with a high enough beam energy, is sufficient to drive the erosion of carbon. Further experiments are required to test the variability in erosion between different instruments/chamber vacuum levels/laboratory humidity levels.

The absorbed current measurement plotted in Figure 8a was recorded at 15kV. At low accelerating voltages, however, absorbed current measurements on the C on Bi samples show increasingly non-linear behaviour, as shown in **Error! Reference source not found.**. At 3.4kV the absorbed current trace shows a prominent and rapid initial rise, which decreases over the first 10 – 15s, transitioning into a linear decrease. At 5kV the initial rise is still apparent but has a markedly lower magnitude. By 7kV only a very small initial kick in the trace is apparent, and this is within the noise level of the data. This non-linearity might be explained by considering the availability of hydrocarbons as a function of irradiation time: As described above, the steady state erosion rate is limited by the surface diffusion rate of hydrocarbons into the beam irradiation zone. When the beam first impacts an area, though, any hydrocarbons already present do not have to diffuse and so could produce a more rapid initial deposition rate. As this local reservoir is exhausted the deposition rate decreases until the surface diffusion limited rate is reached. The implication of the traces in **Error! Reference source not found.** is that this initial rapid deposition rate increases with decreasing accelerating voltage and below 7kV is enough to dominate over the erosion rate until the local reservoir is exhausted.

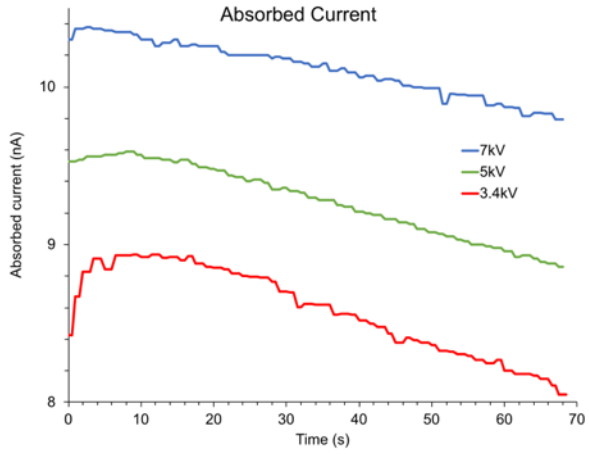

Figure 9 *Absorbed current measurements at 7, 5 and 3.4kV on the '5nm' C on Bi sample. Measurements were recorded at 0.5s intervals for each trace.*

This change in behaviour with accelerating voltage might contribute towards the dramatic increase in scatter in the measured erosion rates below 7kV shown in Figure 6a: A linear extrapolation has been assumed for the TDI measurements but if there is an initial period of rapid deposition a linear fit will underestimate the true steady-state rate of erosion and could produce the spread to lower erosion rates at low accelerating voltages shown in Figure 6a. The C Kα measurements, though, don't give unambiguous indication of this initial increase. **Error! Reference source not found.** shows 2 of the 12 sets of analyses of the

absorbed current and C Kα peak intensities acquired at 3.4kV on the '5nm' C on Bi sample. The absorbed current (black line) shows a substantial and rapid initial increase in both plots. In Figure 10a the 0.5s C Kα measurements (solid red line) shows a slight initial rise. However, this is proportionally a substantially smaller change than in the absorbed current, and the linear fit through the data (red dashed line) does not appear unreasonable. In fact, the very first 0.5s x-ray intensity measurement (710 c/0.5s) very closely agrees with the extrapolated linear trend (720.5 c/0.5s). When the 10s averaged counts (red diamonds) are plotted the dip is more apparent, and agrees quite closely with the 10s averaged absorbed current values (white diamonds). The data set in Figure 10b shows a smaller but still very evident initial increase in absorbed current, but here the x-ray data does not give any indication of non-linear behaviour. The data set plotted in **Error! Reference source not found.**a was selected as showing an initial rise reasonably clearly, but even here the 1σ standard deviation ranges for the x-ray data (shown by the black bars on the red diamonds) overlap with the linear trend line. Comparing the position of the first 10s averaged C Kα data point relative to the linear trend, only 25 of the 48 sets of measurements acquired at 3.4kV showed this first data point below the linear trend. This number would be expected from random variation and thus the x-ray data cannot be concluded to show an initial increase.

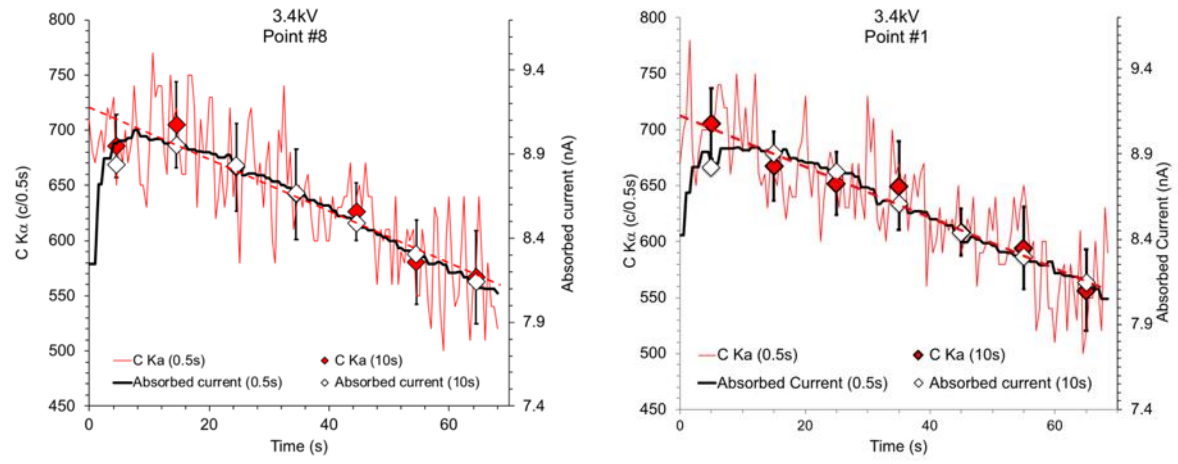

a b

Figure 10 *Comparisons of the absorbed current and C Kα measurements at 3.4kV on the '5nm' C on Bi sample. The black line is the absorbed current measurement, the red solid line is the C Kα intensity, both measured at 0.5s intervals. The diamonds are 10s averaged absorbed current (white) and C Kα intensities (red), the latter with 1σ standard deviation ranges. The red dashed line is the linear fit through the 0.5s absorbed current measurements. In a) the initial increase in the C Kα counts is apparent whilst in b) it is not.*

Regardless of whether or not the x-ray data does initially increase three things can be concluded. Firstly, the absorbed current is either responding disproportionately to a real but small initial contamination deposition or is responding to some other sample property in addition to the coating thickness; Secondly, even if there is an initial deposition, it is too small to be distinguished in the x-ray data and thus cannot be used to explain the increase in scatter seen in the sub-7kV data in Figure 6; Thirdly, the assumption of a linear TDI extrapolation is still valid at low accelerating voltages.

Impact on Quantification

In a previous paper (Matthews et al. 2018) the authors demonstrated that inaccurate determination of a coating thickness can lead to significant errors in substrate quantification. Both attenuation of the primary beam energy and absorption of the generated substrate x-rays by the coating contribute to the reduction in the measured substrate k-ratio. Here, even if the original deposited thickness is assumed to be correctly measured erosion can significantly change that thickness during a static beam analysis.

Using the thin film analysis software GMRFilm (Waldo 1988), the mean C Kα k-ratios were converted into film thicknesses at each interval for each set of analysis conditions. Figure 11 shows the results, plotted as changes in thickness from the extrapolated time-zero values, for the '5nm' coated sample measured using a 25nA 5µm defocussed beam at all six measured accelerating voltages. Whilst there is some spread in the traces, they all show roughly linear decreases in coating thickness. The calculated thickness reductions range from 0.3 to 1.1nm over the 60s analysis period, with the highest erosion rates for the lowest accelerating voltages. These losses represent significant proportions of the 5nm initial coating thickness.

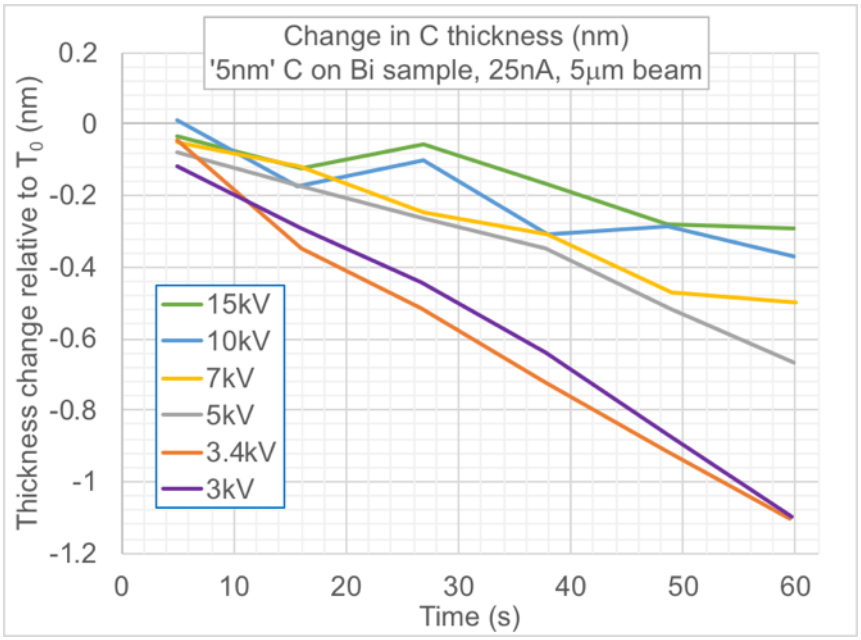

Figure 11 *Change in C coating thickness relative to the extrapolated time-zero value, calculated from the C Kα k-ratios using GMRFilm.*

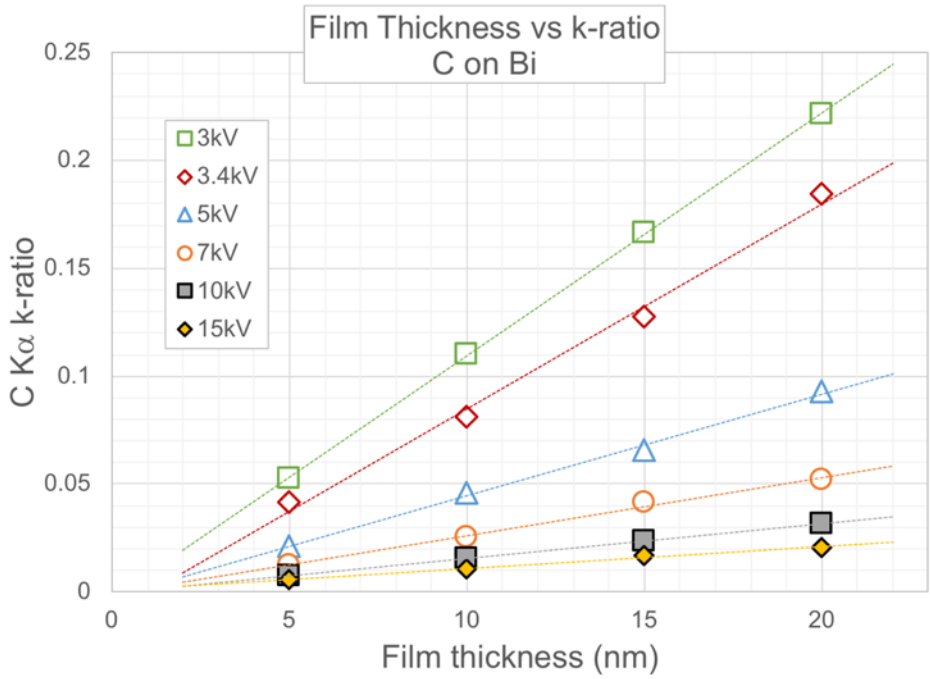

Figure 12 *Plot of C Kα as a function of film thickness. Symbols mark data points calculated using GMRFilm and the lines are straight line fits.*

As was shown for Al and Cu coatings on Bi (Matthews et al. 2018), over the range of voltages and film thicknesses modelled, C Kα k-ratios can be closely approximated as a linear function of film thickness at a given accelerating voltage. This close linear approximation has so far been found to be true for all combinations of coating and substrate materials tested. This shows that, over the range of accelerating voltages and conductive coating thicknesses typically experienced in EPMA, the k-ratios can be assumed to be linear functions of the coating thickness (Figure 12). Calculated errors in k-ratio can therefore be directly translated to errors in film thickness quantification.

Table 2 *Percent difference of uncorrected C Kα k-ratios with respect to TDI-corrected k-ratios [x= 100*(uncorrected-corrected)/corrected].*

shows the percent differences of carbon k-ratios measured without TDI correction from those using TDI correction for analyses with a 25nA fully focussed beam as a function of starting coating thickness and accelerating voltage. The differences increase both with decreasing accelerating voltage and with decreasing starting thickness, from 1.5% for the '20nm' coating at 15kV to 14% for the '5nm' coating at 3kV. It was shown above that the erosion rate is independent of the starting coating thickness. However, since a 1nm loss from a 5nm coat represents 20% decrease, but only a 5% decrease for a 20nm coat the relative differences thus increase with decreasing thickness. The percent differences in the k-ratios can be taken as direct estimates of the analysis errors in the quantification of the coating.

kV \ nm	5.06	10.08	15.10	20.28
3	-13.92	-4.34	-3.46	-4.73
3.4	-10.67	-3.46	-2.59	-2.81
5	-11.47	-2.72	3.67	-0.59

7	-11.09	-6.85	-4.53	-3.75
10	-9.48	-5.94	-6.17	-2.34
15	-6.63	-3.08	-1.52	-1.52

Table 2 *Percent difference of uncorrected C Kα k-ratios with respect to TDI-corrected k-ratios [x= 100*(uncorrected-corrected)/corrected].*

To investigate the propagated effect these errors have on quantification of the substrate a similar treatment is used for the Bi Mα k-ratios in Table 3 Percent difference of uncorrected Bi Mα k-ratios with respect to TDI-corrected k-ratios [x = 100(uncorrected-corrected)/corrected], and overvoltage ratio, U, relative to the Bi M_V absorption edge at 2.5795keV* (Bearden & Burr 1967).

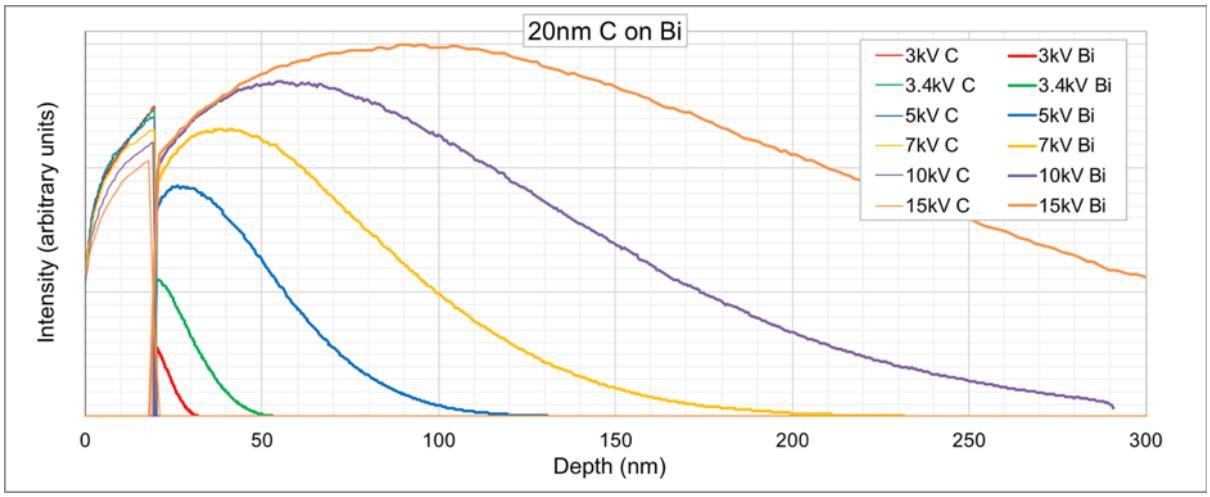

Figure 13 *Intensity versus depth plots as functions of accelerating voltage of C Kα and Bi Mα for a 20nm C on Bi sample. Calculated using Casino v2.51.*

The errors given in Table 2 and Table 3 above are based on calibrations against uncoated reference materials, thus the changes in coating thickness are not balanced against any matching changes in the reference materials. More commonly perhaps, reference materials will also be C coated. If the coating thicknesses are similar, the calibration and measurement conditions are the same (i.e. beam diameter, probe current, counting time), and the accelerating voltage is at least 10kV, then the erosion rates may be expected to be similar for both calibrations and measurements and the errors could largely cancel out. However, as the example in Table 4 shows, even at 10kV the combination of two differing erosion rates under the same analysis conditions can produce percent-level errors. In this example two separate measurements on the '15nm' C coated sample have been used to represent a coated reference material and a sample. Point #1 showed a net decrease in Bi (net C deposition) whilst a net Bi increase was measured for point #11 (c erosion). Using point #1 as the calibration and point #11 as the unknown sample the calculated Bi content is 101wt% without TDI correction but 100wt% with TDI correction. Below 10kV, as we have seen above in Figure 5a, the net erosion/deposition rate can vary significantly and even larger errors can potentially occur if TDI corrections are not used.

'15nm' C, 10kV, 5μm beam	No TDI correction (cps/nA)	TDI corrected (cps/nA)
Point #1 ('Reference')	222.4358	222.9726

Point #11 ('Sample')	224.5011	222.8089
Weight% Bi	**100.93**	**100.01**

Table 4 *Comparison of TDI corrected and uncorrected quantification using two analysis points from the same sample, measured under the same conditions, to demonstrate calibration against a coated reference material. Point #1, used as the calibrating measurement, showed a net Bi decrease during measurement whilst Point #11 showed a net increase.*

Whilst erosion/deposition of carbon coats were only examined on a Bi substrate in this study the principles of the local balance between erosion and deposition, with deposition being limited by surface diffusion and erosion increasing with decreasing accelerating voltage, will apply to all materials. There have been studies which measured contamination rates on different substrates (e.g. (Ranzetta & Scott 1966; Konuma 1983; Ueda & Yoshimura 2004) but very few on erosion rates under EPMA-type conditions. The conditions at which erosion dominates over deposition, however, will depend on the balance between the SE-I and BSE/SE-II emissions. Measurements of SE yields, δ, and BSE coefficients, η, (Reimer & Tollkamp 1980) show that above 10kV both tend to decrease with atomic number but that η decreases faster. Thus, erosion will be expected to dominate at lower flux intensities than has been measured for Bi. Below 10kV the relationship of δ and in particular η against Z does not hold and prediction becomes significantly harder.

Bi is also both thermally and electrically conductive. The erosive effect is therefore not caused by either local electrical or thermal fields. The presence of a negative sub-surface field, as would be expected in an electrically insulating sample, will distort the electron interaction volume closer to the surface. Thus it is expected that the net erosion/deposition will behave as if a lower accelerating voltage is being used.

where the percentage difference of the uncorrected Bi Mα k-ratios relative to the TDI corrected values are given. At accelerating voltages of 5kV or higher the errors are relatively small, less than 1%, for all four coating thicknesses. However, at lower voltages these errors rapidly increase from 4% at 3.4kV to 14 – 20% at 3kV. This sharp increase in error can be linked to the overvoltage ratio, U, which is the ratio between the accelerating voltage and the critical excitation energy of the x-ray being fluoresced. The values of U to excite the Bi M_V shell are shown in the final column in Table 3. At low overvoltages primary electrons entering the sample can only be decelerated a small amount, both from energy losses to the coating (Reed 1975) and within the sample, before they have insufficient remaining energy to fluoresce Bi Mα x-rays. Consequently the depth of x-ray generation becomes very shallow and the coating thickness becomes a more significant proportion of the analysis volume and hence the errors in coating thickness induce proportionally larger errors in the substrate quantification. This is shown graphically in the depth distribution plots in Figure 13. At 5kV Bi accounts for approximately 100nm of the total analysis depth, relative to the 20nm of the C coating. At 3.4kV Bi accounts for only 30nm, and at 3kV it drops to only 10nm, i.e. by this voltage the C coating accounts for 2/3 of the total analysis depth. Between 5kV and 3.4kV the overvoltage ratio drops below 1.5, and this value can perhaps be used as a threshold value for the sensitivity of other systems to this error propagation. Over the range of conditions measured the accelerating voltage is the dominating factor in the magnitude of the error.

kV \ nm	**5.06**	**10.08**	**15.10**	**20.28**	**U**

3	13.96	16.70	17.53	20.16	1.16
3.4	3.98	4.09	3.26	3.97	1.32
5	0.77	0.23	-0.59	-0.06	1.94
7	0.41	0.51	0.05	0.33	2.71
10	0.23	0.19	0.14	0.19	3.88
15	0.14	0.13	0.09	-0.01	5.82

Table 3 *Percent difference of uncorrected Bi Mα k-ratios with respect to TDI-corrected k-ratios [x = 100*(uncorrected-corrected)/corrected], and overvoltage ratio, U, relative to the Bi M_V absorption edge at 2.5795keV* (Bearden & Burr 1967).

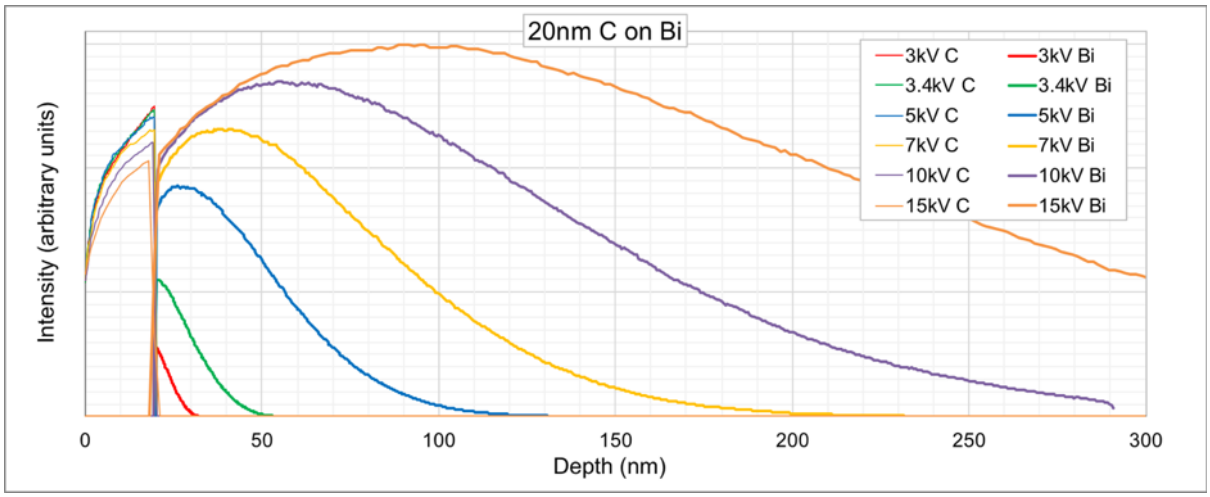

Figure 13 *Intensity versus depth plots as functions of accelerating voltage of C Kα and Bi Mα for a 20nm C on Bi sample. Calculated using Casino v2.51.*

The errors given in Table 2 and Table 3 above are based on calibrations against uncoated reference materials, thus the changes in coating thickness are not balanced against any matching changes in the reference materials. More commonly perhaps, reference materials will also be C coated. If the coating thicknesses are similar, the calibration and measurement conditions are the same (i.e. beam diameter, probe current, counting time), and the accelerating voltage is at least 10kV, then the erosion rates may be expected to be similar for both calibrations and measurements and the errors could largely cancel out. However, as the example in Table 4 shows, even at 10kV the combination of two differing erosion rates under the same analysis conditions can produce percent-level errors. In this example two separate measurements on the '15nm' C coated sample have been used to represent a coated reference material and a sample. Point #1 showed a net decrease in Bi (net C deposition) whilst a net Bi increase was measured for point #11 (c erosion). Using point #1 as the calibration and point #11 as the unknown sample the calculated Bi content is 101wt% without TDI correction but 100wt% with TDI correction. Below 10kV, as we have seen above in Figure 5a, the net erosion/deposition rate can vary significantly and even larger errors can potentially occur if TDI corrections are not used.

'15nm' C, 10kV, 5μm beam	No TDI correction (cps/nA)	TDI corrected (cps/nA)
Point #1 ('Reference')	222.4358	222.9726

Point #11 ('Sample')	224.5011	222.8089
Weight% Bi	**100.93**	**100.01**

Table 4 *Comparison of TDI corrected and uncorrected quantification using two analysis points from the same sample, measured under the same conditions, to demonstrate calibration against a coated reference material. Point #1, used as the calibrating measurement, showed a net Bi decrease during measurement whilst Point #11 showed a net increase.*

Whilst erosion/deposition of carbon coats were only examined on a Bi substrate in this study the principles of the local balance between erosion and deposition, with deposition being limited by surface diffusion and erosion increasing with decreasing accelerating voltage, will apply to all materials. There have been studies which measured contamination rates on different substrates (e.g. (Ranzetta & Scott 1966; Konuma 1983; Ueda & Yoshimura 2004) but very few on erosion rates under EPMA-type conditions. The conditions at which erosion dominates over deposition, however, will depend on the balance between the SE-I and BSE/SE-II emissions. Measurements of SE yields, δ, and BSE coefficients, η, (Reimer & Tollkamp 1980) show that above 10kV both tend to decrease with atomic number but that η decreases faster. Thus, erosion will be expected to dominate at lower flux intensities than has been measured for Bi. Below 10kV the relationship of δ and in particular η against Z does not hold and prediction becomes significantly harder.

Bi is also both thermally and electrically conductive. The erosive effect is therefore not caused by either local electrical or thermal fields. The presence of a negative sub-surface field, as would be expected in an electrically insulating sample, will distort the electron interaction volume closer to the surface. Thus it is expected that the net erosion/deposition will behave as if a lower accelerating voltage is being used.

Conclusions

Whilst carbon contamination in the SEM/EPMA is well recognised, with a disk of contamination forming over an area considerably wider than a static electron beam, the area directly under the beam can exhibit net deposition or erosion, depending on the analysis conditions. Both erosion and deposition rates increase with electron flux density at the sample surface but, since the maximum deposition rate is limited by the surface diffusional supply of source hydrocarbons, the erosion rate rapidly dominates. This results in an rapid change from net deposition to net erosion with increasing flux. For a given primary beam electron flux the erosion rate decreases with increasing accelerating voltage since the emitted electron flux will decrease. For a given voltage erosion can be minimised by reducing the primary beam flux density below a threshold value, either by reducing the beam current or increasing the beam diameter. For the C coated Bi samples analysed in this study at 5kV a flux density of 1nA/nm^2 corresponding to a beam diameter of 10μm was sufficient to minimise erosion. Erosion rates can easily be high enough under relatively normal analysis conditions to significantly reduce the thickness of a Carbon coat during an analysis. At low voltages the issue is exacerbated since the rate of erosion and the proportional impact of the coating on quantification both increase. Even when both samples and reference materials are coated to the same thicknesses it cannot be assumed that both will experience the same net erosion/deposition. Below 10kV the measured erosion/deposition rate also appears to become highly unpredictable. For a given sample analysis point and analysis conditions, though, the rate of erosion or deposition was found

to be constant for at least the 60 – 70s of analysis time. If uncorrected for, errors in the coating thickness determination can range from 1.5% for a starting coating thickness of 20nm analysed at 15kV, to 14% for a 5nm coat analysed at 3kV, the error increasing both with decreasing accelerating voltage and starting coating thickness.

The lateral transition from net erosion under the beam to deposition outside it is rapid. Any instability in the position of the beam during analysis can therefore significantly alter the measured erosion rate, making prediction of the impact on quantification difficult even if the erosion rate has been characterised for a given sample and set of conditions. TDI analysis using a linear extrapolation can be used to correct for both measured erosion or deposition. Absorbed current measurements provide a useful and sensitive check for changes in the coating thickness, and can be acquired simultaneously with the X-ray intensities, without allocating spectrometer time, but cannot easily be used to correct for any changes.

Fortunately, for accelerating voltages of 5kV or higher, the impact on substrate quantification is small, with less than 1% errors. However, below 5kV the propagated error in the Bi Mα measurement rises rapidly, both with decreasing accelerating voltage and increasing starting film thickness, to a 20% error for a 20nm coating at 3kV. The voltage at which the substrate error becomes significant is related to the overvoltages of the elements being measured, and a ratio of 1.5 appears to be a critical threshold for a rapid increase in error. It is therefore recommended that overvoltage ratios of greater than 1.5 are used for substrate quantification.

References

Amman, M., Sleight, J.W., Lombardi, D.R., Welser, R.E. ,Deshpande, M.R. ,Reed, M.A.,& Guido, L.J., 1996. Atomc Force Microscopy Study of Electron Beam Written Contamination Structures. *Journal of Vacuum Science & Technology B*, **14**(1), 54–62.

Bastin, G.F. & Heijligers, H.J.M., 1988. Contamination Phenomena in the Electron Probe Microanalyzer. In Microbeam Analysis, Newbury, D.E. (Ed.), pp. 325–328. San Francisco: San Francisco Press.

Bearden, J.A. & Burr, A.F., 1967. Reevaluation of X-ray atomic energy levels. *Reviews of Modern Physics*, **39**(1), 125–142.

Buse, B., Kearns, S.L., Clapham, C., & Hawley, D., 2016. Decontamination in the Electron Probe Microanalysis with a Peltier-Cooled Cold Finger. *Microscopy and Microanalysis*, **22**(5), 981–986.

Buse, B. & Kearns, S.L., 2015. Importance of Carbon Contamination in High-Resolution (FEG) EPMA of Silicate Minerals. *Microscopy and Microanalysis*, **20**(1), 1–12. Available at: http://www.ncbi.nlm.nih.gov/pubmed/25877617.

Choi, Y.R., Rack, P.D., Randolph, S.J., Smith, D.A., & Joy, D.C., 2006. Pressure effect of growing with electron beam-induced deposition with tungsten hexafluoride and tetraethylorthosilicate precursor. *Scanning*, **28**(6), 311–318.

Demers, H., Poirier-Demers, N., Couture, A.R., Joly, D., Guilmain, M., De Jonge, N., & Drouin, D., 2011. Three-dimensional electron microscopy simulation with the CASINO Monte Carlo software. *Scanning*, **33**(3), 135–146.

van Dorp, W.F., van Someren, B., Hagen, C.W., Kruit, P., & Crozier, P.A., 2005. Approaching the resolution limit of nanometer-scale electron beam-induced deposition. *Nano Letters*, **5**(7), 1303–1307.

Ennos, A.E., 1953. The origin of specimen contamination in the electron microscope. *British Journal of Applied Physics*, **4**(4), 101–106.

Ennos, A.E., 1954. The sources of electron-induced contamination in kinetic vacuum systems. *British Journal of Applied Physics*, **5**(1), 27–31.

Heide, H.G., 1962. The Prevention of Contamination Without Beam Damage to the Specimen. In Electron microscopy : Fifth International Congress for Electron Microscopy, Philadelphia. Breese, S.S., (Ed.), pp. A4-A5. New York: Academic Press.

Hren, J.J., 1979. Barriers to AEM: Contamination and Etching. In Introduction to Analytical Electron Microscopy. Hren, J.J., Goldstein, J.I., & Joy, D., (Eds.), pp. 481–505. New York: Plenum Press.

Isabell, T.C., Fischione, P.E., O'Keefe, C., Guruz, M.U. ,& Dravid, V.P., 1999. Plasma Cleaning and Its Applications for Electron Microscopy. *Microscopy and Microanalysis*, **5**, 126–135.

Kohlmann-von Platen, K.T. & Bruenger, W.H., 1996. Electron-Beam Induced Etching of Resist with Water Vapor as the Etching Medium. *Journal of Vacuum Science & Technology B*, **14**(6), 4262.

Konuma, H., 1983. Rate of carbon contamination on copper, iron and aluminum targets in gas flows by an electron microprobe. *Mikrochimica Acta*, **80**(1–2), 99–108.

Lobo, C.J., Toth, M., Wagner, R., Thiel, B.L., & Lysaght, M., 2008. High resolution radially symmetric nanostructures from simultaneous electron beam induced etching and

deposition. *Nanotechnology*, **19**(2), 025303-1 - 025303-6.

Matthews, M.B., Kearns, S.L. & Buse, B., 2018. The Accuracy of Al and Cu Film Thickness Determinations and the Implications for Electron Probe Microanalysis. *Microscopy and Microanalysis*, **24**(2), 83–92.

Mitchell, D.R.G., 2015. Contamination mitigation strategies for scanning transmission electron microscopy. *Micron*, **73**, 36–46. Available at: http://dx.doi.org/10.1016/j.micron.2015.03.013.

Nielsen, C.H. & Sigurdsson, H., 1981. Quantitative methods for electron microprobe analysis of sodium in natural and synthetic glasses. *American Mineralogist*, **66**(5–6), 547–552.

Pinard, P.T., Schwedt, A., Ramazani, A., Prahl, U., & Richter, S., 2013. Characterization of dual-phase steel microstructure by combined submicrometer EBSD and EPMA carbon measurements. *Microscopy and Microanalysis*, **19**(4), 996–1006. Available at: http://www.ncbi.nlm.nih.gov/pubmed/23742898.

Pinard, P.T., 2016. Thesis: *Electron probe microanalysis of carbon containing steels at a high spatial resolution*. RWTH Aachen University. Available at: http://publications.rwth-aachen.de/record/673259/files/673259.pdf. Retrieved 8 April 2018.

Ranzetta, G.V.T. & Scott, V.D., 1966. Specimen contamination in electron-probe microanalysis and its prevention using a cold trap. *J. Sci. Instrum.*, **43**, 816–819.

Reed, S.J.B., 1975. *Electron Microprobe Analysis*, Cambridge: Cambridge University Press.

Reimer, L. & Tollkamp, C., 1980. Measuring the Backscattering Coefficient and Secondary Electron Yield Inside a Scanning Electron Microscope. *Scanning*, **3**, 35–39.

Reimer, L. & Wachter, M., 1978. Contribution to the Contamination Problem in Transmission Electron Microscopy. *Ultramicroscopy*, **3**, 169–174.

Shimojo, M., Mitsuishi, K. Tameiki, A. & Furuya, K., 2004. Electron induced nanodeposition of tungsten using field emission scanning and transmission electron microscopes. *Journal of Vacuum Science & Technology B*, **22**(2), 742–746. Available at: http://scitation.aip.org/content/avs/journal/jvstb/22/2/10.1116/1.1688349.

Silvis-Cividjian, N., Hagen, C.W., & Kruit, P., 2002. The role of secondary electrons in electron-beam-induced-deposition spatial resolution. *Microelectronic Engineering*, **61–62**, 693–699. Available at: http://www.sciencedirect.com/science/article/pii/S0167931702005154.

Stormer, J.C., Pierson, M.L. & Tacker, R.C., 1993. Variation of F and Cl X-ray intensity due to anisotropic diffusion in apatite during electron microprobe analysis. *American Mineralogist*, **78**(5–6), 641–648.

Tanaka, M., Shimojo, M., Han, M., Mitsuishi, K., & Furuya, K., 2005. Ultimate sized nano-dots formed by electron beam-induced deposition using an ultrahigh vacuum transmission electron microscope. *Surface and Interface Analysis*, **37**(2), 261–264.

Toth, M., Lobo, C.J., Hartigan, G., & Ralph Knowles, W., 2007. Electron flux controlled switching between electron beam induced etching and deposition. *Journal of Applied Physics*, **101**(5), 54309-1 - 54309–6.

Ueda, K. & Yoshimura, M., 2004. Fabrication of nanofigures by focused electron beam-induced deposition. *Thin Solid Films*, **464–465**, 331–334.

Utke, I., Hoffmann, P. & Melngailis, J., 2008. Gas-assisted focused electron beam and ion beam processing and fabrication. *Journal of Vacuum Science & Technology B:*

Microelectronics and Nanometer Structures, **26**(4), 1197. Available at: http://scitation.aip.org/content/avs/journal/jvstb/26/4/10.1116/1.2955728.

Waldo, R.A., 1988. An Iteration Procedure to Calculate Film Compositions and Thicknesses in Electron-Probe Microanalysis. In Microbeam Analysis, Newbury, D.E. (Ed.), pp. 310–314. San Francisco: San Francisco Press.